val Research Laboratory
ington, DC 20375-5000

NRL Memorandum Report 6746

Time-Dependent Multimode Simulation of Gyrotron Oscillators

A. W. FLIFLET, R. C. LEE,* S. H. GOLD, W. M. MANHEIMER AND E. OTT†

Beam Physics Branch
Plasma Physics Division

** Jaycor, Inc.,*
Vienna, VA 22184

† Laboratory of Plasma Research,
University of Maryland,
College Park, MD 20742

November 21, 1990

REPORT DOCUMENTATION PAGE

Form Approved
OMB No. 0704-0188

1. AGENCY USE ONLY (Leave blank)	2. REPORT DATE	3. REPORT TYPE AND DATES COVERED
	1990 November 21	Interim

4. TITLE AND SUBTITLE
Time-Dependent Multimode Simulation of Gyrotron Oscillators

5. FUNDING NUMBERS
RRO-11-09-4J

47-M003-A-0

6. AUTHOR(S)
A. W. Fliflet, R. C. Lee,* S. H. Gold, W. M. Manheimer and E. Ott†

7. PERFORMING ORGANIZATION NAME(S) AND ADDRESS(ES)
NRL
Washington, DC 20375-5000

8. PERFORMING ORGANIZATION REPORT NUMBER
NRL Memorandum Report 6746

9. SPONSORING/MONITORING AGENCY NAME(S) AND ADDRESS(ES)
Office of Naval Research
Arlington, VA 22217

10. SPONSORING/MONITORING AGENCY REPORT NUMBER

11. SUPPLEMENTARY NOTES
* Jaycor, Inc., Vienna, Va 22182
† Laboratory of Plasma Research, University of Maryland, College Park, MD 20742

12a. DISTRIBUTION/AVAILABILITY STATEMENT
Approved for public release; distribution unlimited.

12b. DISTRIBUTION CODE

13. ABSTRACT (Maximum 200 words)

High power gyrotrons, including both CW and high peak power configurations, are increasingly designed to operate in high mode density regimes. It has been observed that operation is often single-moded even for cavities with dense mode spectra, but the mode density does affect the gyrotron efficiency and the available operating modes. Multimode effects have been studied extensively for the quasi-optical gyrotron but there has been less progress on fully nonlinear formulations for conventional waveguide cavity gyrotrons which involve different transverse modes with irregularly spaced frequencies and unequal coupling impedances. A time-dependent, nonlinear, multimode theory of gyrotrons has been recently developed along with a computer code to carry out the numerical calculations. The code has been used to simulate the operation of a CW-relevant 140 GHz gyrotron experiment carried out at MIT and the 750 kV, 35 GHz intense-beam gyrotron experiment at NRL. The MIT gyrotron involves competition between two transverse modes: the TE_{03} and TE_{23} modes. The NRL gyrotron involves competition between TE_{m2} modes and is an example of a three-mode interaction.

14. SUBJECT TERMS	15. NUMBER OF PAGES
Multi-mode Simulation Gyrotron	36
	16. PRICE CODE

17. SECURITY CLASSIFICATION OF REPORT	18. SECURITY CLASSIFICATION OF THIS PAGE	19. SECURITY CLASSIFICATION OF ABSTRACT	20. LIMITATION OF ABSTRACT
UNCLASSIFIED	UNCLASSIFIED	UNCLASSIFIED	SAR

NSN 7540-01-280-5500

Standard Form 298 (Rev 2-89)
Prescribed by ANSI Std 239-18
298-102

CONTENTS

TIME-DEPENDENT MULTIMODE SIMULATION OF GYROTRON OSCILLATORS

I Introduction

High power gyrotrons, including both CW and high peak power configurations, are increasingly designed to operate in high mode density regimes. For example, at NRL high voltage gyrotrons have produced powers approaching 100 MW in the $TE_{12,2}$ transverse mode of the cylindrical cavity at a frequency of 49 GHz,[1] and at MIT CW-relevant gyrotrons have produced 100's of kW in modes as high as the $TE_{27,6}$ mode at a frequency of 327 GHz.[2] It has been observed that operation is often single-moded even for cavities with dense mode spectra, but the mode density does affect the efficiency and the accessible operating modes. Multimode effects have received considerable theoretical attention, but there has been relatively little work on fully nonlinear formulations because of the extensive computations required to obtain results. The calculation of multimode effects in waveguide cavity gyrotrons is complicated by the unequal coupling impedances and irregularly-spaced frequencies of the transverse modes. In this paper a time-dependent, nonlinear, multimode theory of waveguide-cavity gyrotron oscillators is formulated and numerical results are presented for the simulation of two gyrotron configurations.

Early work on the theory of multimode oscillations of triode oscillators was carried out by van der Pol based on a lumped circuit element approach.[3] A multimode theory of lasers was obtained by Lamb.[4,5] The multimode laser theory was adapted to the multimode operation of gyrotrons by Nusinovich and co-workers.[6,7] A time-dependent multimode theory of quasi-optical gyrotrons has been developed by Bondeson et al.[9] The stability of single-mode gyrotron operation with respect to parasitic oscillations has been examined by Antonsen et al.,[8] Dumbrajs et al.[10], and by Borie and Jödicke.[11] Multimode effects in gyrotron have also been studied using a particle-in-cell (PIC) code by Lin and co-workers.[12]

In this work the problem of multimode oscillations in gyrotrons is investigated using a theory similar in form to that used in the study of multimode lasers.[5] The approach involves solving the following coupled, nonlinear, time-dependent equations, derived in

Manuscript approved September 12, 1990.

Section II, for the mode amplitudes (a_n) and phases (ψ_n) of the form:

$$\frac{da_n}{dt} + \frac{\omega_0 a_n}{2Q_n} = -\frac{\omega_r}{2\varepsilon_0}\mathrm{Im}\mathcal{P}_n(t) \quad (1)$$

$$\frac{d\psi_n}{dt} + \omega_0 = \omega_{n0} - \frac{\omega_0}{2\varepsilon_0 a_n}\mathrm{Re}\mathcal{P}_n(t), \quad (2)$$

where $\mathcal{P}_n$ is the complex, slow-time-scale component of the electron beam polarization for the mode n, ω_{n0} is the mode cold-cavity eigenfrequency, ω_0 is a nearby reference frequency, Q_n is the mode quality factor, and ε_0 is the permittivity of free space. Equations of this form are well known from the semiclassical theory of lasers[4,5] and have been applied to gyrotrons by Nusinovich and coworkers. In most previous gyrotron applications, the above equations have been solved in the same manner as for lasers by expanding the polarization in powers of the mode amplitude and neglecting higher order terms—usually above third order. Such perturbation expansions should be valid for beam currents near the oscillation threshold, but the accuracy is open to question at currents 10–20 times the threshold value which are typically needed for efficent, high power operation. For this reason, a fully nonlinear approach has been adopted in the present formulation.

The results of calculations are presented for two experimental gyrotron configurations: a 140 GHz, 65 kV, TE_{03} mode gyrotron[13] and a 35 GHz, TE_{62} mode intense-beam gyrotron.[1] The former represents a useful benchmark because very detailed experimental data is available.[13] The latter experiment is in an interesting high peak power, short pulse regime for which the experimental data is less extensive. It has also been simulated by Lin et al.[12] using a multimode particle-in-cell code, and it is interesting to compare the different theoretical approaches.

II Theory

Consider a gyrotron with a cylindrical resonator and a thin annular beam. The electrons follow helical trajectories in the applied axial magnetic field about guiding centers located at a distance R_0 from the symmetry axis. The beam interacts with one or more resonator modes, which are assumed to have closely-spaced oscillation frequencies. The electron beam

and cavity cross sectional geometries are shown in Fig. 1. It is convenient to look at time-dependent effects which remain after a reference frequency ω_0 has been factored out. These effects are characterized by time-scales which are much longer than a wave period and are incorporated in the complex mode amplitudes $A_n(z,t)$ which also describe the mode spatial dependence in the z-direction. The total transverse electric field is expressed in the form:

$$\vec{E} = \sum_{n=1}^{N} A_n(z,t)\,\vec{e}_n(r,\theta;z)\,e^{-i\omega_0 t} \tag{3}$$

where $\vec{e}_n = \hat{z} \times \vec{\nabla}_t \Psi$ is the waveguide transverse-mode vector function and Ψ is the corresponding scalar mode function which satisfies a Helmholtz equation with respect to the transverse coordinates.[14] N is the number of interacting modes. The transverse electric field satisfies the wave equation:

$$\nabla^2 \vec{E}_t - \frac{1}{c^2}\frac{\partial^2 \vec{E}_t}{\partial t^2} = \mu_0 \frac{\partial \vec{J}_t}{\partial t} \tag{4}$$

where $\vec{J}_t$ is the transverse AC current density, c is the speed of light, and μ_0 is the permeability of free space. MKS units are used throughout except as noted. Substituting Eq.(3) into Eq.(4), integrating over the resonator cross section, and noting that $\partial A_n/\partial t \ll \omega_0 A_n$, one obtains:

$$\left[\frac{\partial^2}{\partial z^2} + \frac{\omega_0^2 - \omega_{nc}^2}{c^2} + 2i\frac{\omega_0}{c^2}\frac{\partial}{\partial t}\right] A_n(z,t) = -i\mu_0\omega_0 \int da \vec{e}_n^{\,*} \cdot \vec{J}_\omega \tag{5}$$

where derivatives with respect to z of the transverse vector function have been neglected, and $\omega_{nc} = \omega_{nc}(z)$ is the local mode cutoff frequency, which may depend on the axial position. In deriving Eq.(5) the RF current density has been expressed in the approximate form:[15]

$$\vec{J}_t = \vec{J}_\omega e^{-i\omega_0 t} \tag{6}$$

where

$$\vec{J}_\omega = \int_0^{2\pi} d(\omega_0 t)\vec{J}_t e^{i\omega_0 t} \tag{7}$$

To obtain slow-time-scale equations for a gyrotron oscillator, multiply Eq.(5) by A_n^* and multiply the complex conjugate of Eq.(5) by A_n. Then first add and then subtract the

resulting equations, and integrate the sum or difference over the axial extent of the cavity. The difference leads to:

$$\int_0^L dz \left[A_n^* \frac{\partial^2 A_n}{\partial z^2} - A_n \frac{\partial^2 A_n^*}{\partial z^2} + 2i \frac{\omega_0}{c^2} \frac{\partial |A_n|^2}{\partial t} \right] = -i\mu_0 \omega_0 \int_V da\, dz \left[A_n^* \vec{e}^{\,*} \cdot \vec{J}_\omega + A_n \vec{e} \cdot \vec{J}_\omega^* \right], \tag{8}$$

where V denotes integration over the cavity volume. The sum leads to:

$$\int_0^L dz \left[A_n^* \frac{\partial^2 A_n}{\partial z^2} + A_n \frac{\partial^2 A_n^*}{\partial z^2} + 2 \frac{\omega_0^2 - \omega_{cn}^2}{c^2} A_n A_n^* + 2i \frac{\omega_0}{c^2} \left(A_n^* \frac{\partial A_n}{\partial t} - A_n \frac{\partial A_n^*}{\partial t} \right) \right] = -i\mu_0 \omega_0 \int_V da\, dz \left[A_n^* \vec{e}^{\,*} \cdot \vec{J}_\omega - A_n \vec{e} \cdot \vec{J}_\omega^* \right], \tag{9}$$

As will be shown, Eq.(8) leads to an equation for the amplitude of the mode n, and Eq.(9) leads to an equation for the mode phase. Integrating the first two terms on the right-hand side of these equations by parts leads to:

$$\left(A_n^* \frac{\partial A_n}{\partial z} - A_n \frac{\partial A_n^*}{\partial z} \right) \Bigg|_0^L + 2i \frac{\omega_0}{c^2} \int_0^L dz \frac{\partial |A_n|^2}{\partial t} = -i\mu_0 \omega_0 \int_V da\, dz \left[A_n^* \vec{e}_n^{\,*} \cdot \vec{J}_\omega + A_n \vec{e}_n \cdot \vec{J}_\omega^* \right], \tag{10}$$

and

$$\frac{\partial |A_n^2|}{\partial z} \Bigg|_0^L + \int_0^L dz \left[-2 \left| \frac{\partial A_n}{\partial z} \right|^2 + \frac{(\omega_0^2 - \omega_{cn}^2)}{c^2} |A_n|^2 + 2i \frac{\omega_0}{c^2} \left(A_n^* \frac{\partial A_n}{\partial t} - A_n \frac{\partial A_n^*}{\partial t} \right) \right] = -i\mu_0 \omega_0 \int_V da\, dz \left[A_n^* \vec{e}_n^{\,*} \cdot \vec{J}_\omega - A_n \vec{e}_n \cdot \vec{J}_\omega^* \right] \tag{11}$$

respectively. As discussed in previous work,[16] the first term on the left-hand side of Eq.(11) is a boundary term which vanishes for a free running oscillator because $A_n \to 0$ at the cavity input ($z = 0$) and $|A_n|$ = constant at the cavity output ($z = L$) when there is only an outgoing wave. The boundary term in Eq.(10) corresponds to the net power flow from the cavity in the mode n. At the cavity output the mode amplitude function has the

form of an outgoing wave with amplitude A_{nL} and wavenumber k_{nz}, i.e.,

$$A_n\left(z=L,t\right)=a_{nL}\left(t\right)e^{i[k_{nz}z-\psi_n(t)]}, \tag{12}$$

where ψ_n is a slowly varying mode phase parameter. Thus for a free-running oscillator, the boundary term in Eq.(10) can be written as:

$$\left(A_n^*\frac{\partial A_n}{\partial z}-A_n\frac{\partial A_n^*}{\partial z}\right)\Bigg|_0^L=2ik_{nz}a_{nL}^2\left(t\right) \tag{13}$$

The mode amplitude function inside the cavity is approximated by the separable form:

$$A_n(z,t)=a_n(t)e^{-i\psi_n(t)}h(z), \tag{14}$$

where $h_n(z)$ is an axial profile function which satisfies the Helmholtz equation:

$$\left[\frac{d^2}{dz^2}+k_{nz}^2\right]h_n(z)=0 \tag{15}$$

or approximates the solution of this equation. In this formulation, the function $P_n=\vec{e}_n h_n$ approximates an eigenfunction of the gyrotron resonator with eigenfrequency ω_{n0} and beam loading effects on the mode axial profile are neglected. Possible choices for h_n for the lowest order axial mode include the sinusoidal profile: $h(z)=\sin(k_z z)$ where $k_z=\pi/L$ and the Gaussian profile: $h(z)=\exp[-(\kappa_z z)^2]$, centered at the cavity midpoint, where $\kappa=2/L$ is the effective axial wave number.[17] The sinusoidal profile corresponds to a closed cylindrical cavity whereas the Gaussian profile approximates the fields in a tapered waveguide cavity. In the remainder of this paper the mode subscript will be dropped from the profile function.

The mode amplitude in the cavity can be related to the mode amplitude at the cavity output via the output Q factor according to:

$$a_{nL}(t)=\left[\frac{W}{k_{nz}Q_n}\right]^{1/2}\frac{\omega_0}{c}a_n(t). \tag{16}$$

Substituting Eqs.(13), (14), and (16) into Eq.(10), and Eqs.(14) and (16) into Eq.(11), applying Eq.(15), and carrying out the axial integrations on the left-hand side of Eqs.(11) and (10) leads to the free-running oscillator equations for the mode amplitude and phase,

Eqs. (1) and (2) given in Section I and repeated below:

$$\frac{da_n}{dt} + \frac{\omega_0 a_n}{2Q_n} = -\frac{\omega_0}{2\varepsilon_0}\mathrm{Im}\mathcal{P}_n(t) \tag{17}$$

$$\frac{d\psi_n}{dt} + \omega_0 = \omega_{n0} - \frac{\omega_0}{2\varepsilon_0 a_n}\mathrm{Re}\mathcal{P}_n(t), \tag{18}$$

where

$$\mathcal{P}_n(t) = \frac{\imath}{W}\int_V da\, dz\; h(z)\vec{e}_n^{\,*}\cdot\vec{J}_\omega e^{i\psi_n}, \tag{19}$$

is the complex, slow-time-scale component of the electron beam polarization for the mode n,

$$W = \int_0^L dz\,|h(z)|^2, \tag{20}$$

ε_0 is the free space permittivity, and the approximation: $\omega_0^2 - \omega_{n0}^2 \approx 2\omega_0(\omega_0 - \omega_{n0})$ has been used. Performing the integral in Eq.(20) leads to $W = L/2$ for the sinusoidal profile, and $W \approx [\pi/2]^{1/2}\, L/2$ for a truncated Gaussian profile.

As an aside, the mode polarization is related to the mode susceptibility according to:

$$\mathcal{P}_n = \varepsilon_0\chi_n a_n = \varepsilon_0(\chi_n' + \imath\chi_n'')\, a_n \tag{21}$$

The mode amplitude and phase equation can be expressed in terms of the susceptibility according to:

$$\frac{da_n}{dt} + \frac{\omega_0}{2Q_n}a_n = -\frac{\omega_0}{2}a_n\chi_n'' \tag{22}$$

$$\frac{d\psi_n}{dt} + \omega_0 = \omega_{n0} - \frac{\omega_0}{2}\chi_n'. \tag{23}$$

Eq.(23) shows that the mode oscillation frequency is shifted from the cold-cavity frequency by $-\frac{1}{2}\omega_0\chi_n'$.

The value of the mode polarization at the time t depends on the motion of electrons which entered the cavity between the times t and $t - L/v_z$. Thus Eqs.(1) and (2) are nonlocal integro-differential equations. To calculate the AC current density, the interaction with the electron beam is treated in the single-particle approximation. The general time-dependent problem can be simplified by using the fact that the characteristic rise-time of

fields in the resonator is much longer than the electron transit time in the cavity as well as the wave period. In this case one can use a quasi-steady-state approximation in which the electron trajectories are calculated for RF modes with fixed amplitude and linearized phase: $\tilde{\psi}_n \approx \psi_n(t_0) + \psi_n'(t_0)(t - t_0)$. The slow-time-scale nonlinear equations-of-motion for an electron in a thin annular beam immersed in a tapered magnetic field and interacting at a particular harmonic with several circularly polarized TE modes (including all field components) are readily deduced from previous steady-state, single-mode analyses and are given by:

$$\frac{du_t}{d\bar{z}} = -\frac{\gamma}{u_z}\sum_{n=1}^{N} f_n J_s'\left(\bar{k}_t\bar{r}_L\right)\mathrm{Re}\left\{\left(h + i\frac{u_z}{\gamma\bar{\omega}_0}\frac{dh}{d\bar{z}}\right)e^{-\left[\Lambda+\tilde{\psi}_n+(m_n-s)\Theta_0\right]}\right\} + \frac{u_t}{2\bar{\Omega}_z}\frac{d\bar{\Omega}_z}{d\bar{z}} \tag{24}$$

$$\frac{d\Lambda}{d\bar{z}} = \bar{\omega}_0\left(1 - \frac{s\bar{\Omega}_z\gamma_0}{\bar{\omega}_0\gamma}\right) - \frac{s\gamma}{u_z u_t} \sum_{n=1}^{N} f_n \frac{sJ_s'\left(\bar{k}_{nt}\bar{r}_L\right)}{\bar{k}_t\bar{r}_L}\mathrm{Re}\left\{\left(h + i\frac{u_z}{\gamma\bar{\omega}_0}\frac{dh}{d\bar{z}} - \frac{\bar{\omega}_{n0}^2 u_t^2}{s\bar{\Omega}\bar{\omega}_0\gamma}h\right)e^{-\left[\Lambda+\tilde{\psi}_n+(m_n-s)\Theta_0\right]}\right\} \tag{25}$$

$$\frac{du_z}{d\bar{z}} = \frac{u_t}{u_z\bar{\omega}_0}\sum_{n=1}^{N} f_n J_s'\left(\bar{k}_{nt}\bar{r}_L\right)\mathrm{Re}\left\{i\frac{dh}{d\bar{z}}e^{-\left[\Lambda+\tilde{\psi}_n+(m_n-s)\Theta_0\right]}\right\} - \frac{u_t^2}{2u_z\bar{\Omega}_z}\frac{d\bar{\Omega}_z}{d\bar{z}} \tag{26}$$

where $u_t = \gamma v_t/c$ is the normalized transverse momentum amplitude, $u_z = \gamma v_z/c$ is the normalized axial momentum (v_t and v_z denote the electron transverse and axial velocities, respectively),

$$\Lambda = (\omega_0 - s\Omega/\gamma_0)\, z/v_z + \omega_0 t_0 - s\phi \tag{27}$$

gives the slow variation in the transverse momentum azimuthal phase relative to the reference wave phase, s is the harmonic number, γ (γ_0) is the (initial) relativistic mass ratio which is given by:

$$\gamma = \left(1 + u_t^2 + u_z^2\right)^{1/2}, \tag{28}$$

k_{nt} is the mode transverse wave number, r_L is the Larmor radius of the orbit, $J_s(J_s')$ is (the derivative of) a regular Bessel function, Ω_z is the nonrelativistic cyclotron frequency for

the z-component of the magnetic field, and f_n is the amplitude of a mode with azimuthal dependence $e^{im_n\theta}$ at the time t_0. The mode amplitude for $m_n > 0$ is normalized according to:

$$f_n = \frac{|e|}{m_0 c^2} x'_n C_n J_{m_n - s}(k_{nt} R_0)\, a_n(t_0) \tag{29}$$

The sign of m_n determines the direction of mode rotation. The mode rotates in the same direction as the electron cyclotron motion for $m_n > 0$, and in the opposite direction for $m_n < 0$. The normalized wave amplitude for $m_n < 0$ is given by Eq.(29) with m_n replaced by $|m_n|$ and $J_{m-s}(k_{nt}R_0)$ replaced by $(-1)^s J_{|m|+s}(k_{nt}R_0)$. Quantities with an overbar have been normalized according to: $\bar{z} = z/r_w$, $\bar{r}_L = r_L/r_w$, $\bar{\Omega} = \Omega r_w/c$, $\bar{\omega}_0 = \omega_0 r_w/c$, and $\bar{k}_{nt} = k_{nt} r_w$. R_0 and Θ_0 denote the electron orbit guiding center radius and azimuthal angle, $|e|$ is the electron charge, m_0 is the electron rest mass, m_n is the azimuthal index for the mode n, x'_n is a zero of J'_{m_n}, r_w is an arbitrary normalization radius, and ϕ gives the slow variation in the transverse momentum phase relative to the cyclotron motion. The linearized mode phase parameter is given by:

$$\tilde{\psi}_n(z) = \psi_n(t_0) + (d\psi_n/dt)|_{t_0}\, z/v_z \tag{30}$$

The transverse TE mode normalization coefficient

$$C_n = \left\{ \left[\pi \left(x'^2_{m_n l_n} - m_n^2 \right) \right]^{1/2} J_{m_n}\left(x'_{m_n l_n} \right) \right\}^{-1}. \tag{31}$$

The AC current density is obtained by integrating Eqs.(24)–(25) for an appropriate set of initial conditions at the cavity input $z = 0$. For a thin annular beam the transverse AC current density is given by:

$$\vec{J}_t = -\frac{I_0}{v_z}\vec{v}_t. \tag{32}$$

Substitution of Eqs.(7) and (6) into Eq.(19) and using the prescription developed in previous work,[15] Eqs.(1) and (2) for the mode amplitude and phase can be rewritten as:

$$\frac{df_n}{d\tau} = -\frac{f_n}{2Q_n} + \tilde{I}_n \int_0^{\bar{L}} d\bar{z}\; h(\bar{z}) \left\langle J'_s(k_{nt} r_L) \frac{u_t}{u_z} \cos\left[\Lambda + \tilde{\psi}_n - (m_n - s)\,\Theta_0 \right] \right\rangle_{\Lambda_0, \Theta_0} \tag{33}$$

$$\frac{d\psi_n}{d\tau} = -\frac{\omega_0 - \omega_{no}}{\omega_0}$$
$$-\tilde{I}_n \int_0^L d\bar{z}\; h(\bar{z}) \left\langle J_s'(k_{nt} r_L) \frac{u_t}{u_z} \sin\left[\Lambda + \tilde{\psi}_n - (m_n - s)\,\Theta_0\right] \right\rangle_{\Lambda_0,\Theta_0} \tag{34}$$

where $\langle\ \rangle_{\Lambda_0,\Theta_0}$ denotes the average with respect to the initial momentum phases and guiding center angles of the electrons, and $\bar{L}$ is the normalized interaction length. The normalized current is given by:

$$\tilde{I}_n = \frac{|e| Z_0}{m_0 c^2 \bar{\omega}_0} \frac{J_{m_n - s}^2(k_{nt} R_0)}{\pi \left(1 - m_n^2/x_{m_n l_n}'^2\right) J_{m_n}^2(x_{m_n l_n}') \bar{W}} I_0 \tag{35}$$

where I_o is the DC beam current and the free-space impedance $Z_0 = 377$ ohms. The numerical calculations can be simplified for low-order harmonic interactions by noting that the argument of the Bessel function J_s (J_s') which occurs in the equations-of-motion and the mode amplitude and phase source terms can be expressed as:

$$k_{nt} r_L \approx s v_t / c, \tag{36}$$

and therefore these Bessel functions can be replaced by their small argument expansion with little loss of accuracy.

The time-dependent simulation is initiated by assigning a small initial amplitude and arbitrary phase to a set of modes which may participate in the interaction. The corresponding induced AC current density is obtained by integrating the equations-of-motion [Eqs.(24)–(26)] and is used to construct the source terms in Eqs.(33) and (34). Eqs.(33) and (34) can then be integrated a single time step and the process repeated. The initial conditions for the equations-of-motion for a cold, phase-mixed electron beam are: $u_t(0) = u_{t_0}, u_z(0) = u_{z_0}$, a fixed guiding-center radius R_0, and $\Lambda(0) = \Lambda_0$ and Θ_0 are uniformly distributed in the interval $[0, 2\pi]$. The interaction efficiency is given by:

$$\eta = \frac{\gamma_0 - \langle \gamma(z = L) \rangle_{\Lambda_0,\Theta_0}}{\gamma_0 - 1} \tag{37}$$

and the output power in the mode n is given by:

$$P_n(\tau) = \frac{\pi m_0^2 c^4}{2 Z_0 |e|^2} \frac{\left(1 - m_n^2/x_{m_n l_n}'^2\right) J_{m_n}^2(x_{m_n l_n}')}{Q_n J_{m_n \mp s}^2(k_{nt} R_0)} \bar{\omega}_0 \bar{W} |f_n(\tau)|^2 \tag{38}$$

for modes with $m_n = \pm|m_n|$, respectively.

For comparison with other work it is useful to introduce the following normalized parameters which are often used in gyrotron analysis[18]:

$$F_n = \frac{1}{\gamma_0 \beta_{t0}^{4-s}} \left(\frac{s^s}{2^{s-1} s!} \right) \frac{f_n}{x'_{m_n l_n}} \tag{39}$$

$$\mu = \pi \frac{\beta_{to}^2}{\beta_{z0}} \frac{L}{\lambda} \tag{40}$$

$$\Delta_n = \frac{2}{\beta_{t0}^2} \left(1 - \frac{s\Omega_{z0}}{\omega_{n0}\gamma_0} \right) \tag{41}$$

where F_n is the normalized mode amplitude, μ is the normalized interaction length, and Δ_n is a mode detuning parameter. In analyzing multimode systems Antonsen et al. have introduced the alternative amplitude parameter $\epsilon_n = F_n \mu$ and the kinematic phase-slip parameter $\delta_n = \Delta_n \mu / 2$.[8] The latter parameters are useful for comparison with experimental data because they are less sensitive to the beam pitch ratio $\alpha = v_t / v_z$ than the former set of normalized parameters. Antonsen et al. also introduce the mode density parameter: $T_0 = T_R / T_p$ where T_R is the repetition time for the quasi-periodic multimode RF field, and $T_p = L/(2v_{z0})$ is half the electron beam transit time in the cavity.

III Calculations and Results

Multimode calculations have been carried out for two gyrotron configurations: a 64 kV, $TE_{0,3,1}$ mode gyrotron designed to operate at 140 GHz; and a 750 kV, $TE_{6,2,1}$ mode gyrotron designed to operate at 35 GHz. The former was investigated experimentally at MIT[2] and the latter was investigated experimentally at NRL.[1] Operation of the $TE_{0,3,1}$ mode gyrotron is limited by competition from the $TE_{2,3,1}$ mode, whereas operation of the $TE_{6,2,1}$ mode gyrotron is limited mainly by competition from other $TE_{m,2,1}$ modes. The highly accurate data from the thermionic cathode, repetitively-pulsed MIT experiment provides an opportunity to benchmark the multimode theory on a relatively simple, well-characterized configuration.

The numerical integrations were carried out using a fourth-order Runga-Kutta algorithm.[19]

Twelve phases were used in the average over Λ_0 and twelve angles were used in the average over Θ_0. Fifty points were used in the axial integrations. The results were found to be insensitive to increasing the number of points used in these averages and integrations. These numbers have also been found to provide adequate numerical accuracy in previous calculations of the steady-state, single-mode efficiency of free-running oscillators. The time step for multimode calculations must generally be much smaller than for the corresponding single-mode calculation. This is especially true for systems with relatively large mode frequency separations because in this case the reference frequency will be significantly different from some of the mode frequencies so that the phase time derivatives for these modes will be large. This necessitates a small time step for accurate numerical integration. In the NRL gyrotron simulation the mode separation was about 8 GHz and the time step was 5 psec. The time step used in the MIT gyrotron simulation was 20 psec. The sinusoidal axial profile was used in the calculations reported here. As shown in previous work,[15] the sinusoidal profile leads to lower peak theoretical nonlinear efficiencies (by $\sim 20\%$) than either the Gaussian or the more accurate self-consistent profile;[15] however, parameter trends should be given correctly.

III-A $TE_{0,3,1}$ Mode Gyrotron Results

A CW-relevant gyrotron designed to operate in the $TE_{0,3,1}$ mode at 140 GHz has been extensively tested at MIT by Kreischer, Temkin and co-workers.[13] TE_{0n} type modes are desirable for their low ohmic losses, but operation is limited by competition from the TE_{2n} modes—in this case the $TE_{\pm 2,3,1}$ modes which have a resonant frequency near 137 GHz. The gyrotron design parameters, which were used in the calculations, include: an output Q factor of 1500, a normalized cavity length $L/\lambda = 7.1$, a maximum cavity wall radius $r_w = 0.348$ cm, a beam guiding center radius $R_0 = 0.182$ cm, and a beam velocity pitch ratio $\alpha = 1.5$. Calculations were carried out as a function of magnetic field and beam current for a beam energy of 64 keV. To approximate the finite risetime of the electron gun voltage, the beam energy was ramped up, linearly, from 44 keV to the maximum

value, 64 keV, during the first 5 nsec of the simulation. Consistent with temperature-limited emission operation of the cathode, the maximum beam current was used from the beginning of the simulations. The beam velocity pitch ratio was increased linearly during the beam energy ramp-up.

The time evolution of the mode output powers is shown for a magnetic field of 5.38 T and a current of 4 A in Fig. 2. As shown in the figure, the TE_{03} mode turns on first during the beam energy ramp, followed by the onset of the $TE_{\pm 2,3}$ modes near the end of the ramp. The reason for this behavior is shown by Fig. 3 which plots Q times the threshold beam power for the TE_{03} and TE_{23} modes as a function of beam voltage as well as the corresponding Q times beam power. The threshold for excitation of the TE_{03} mode occurs at about 46 kV, or early in the voltage rise. In comparison, the threshold voltage for the $TE_{\pm 2,3}$ modes is about 55 kV. At this magnetic field the $TE_{\pm 2,3}$ modes ultimately supress the TE_{03} mode, thus limiting the efficiency optimization of this mode by magnetic field detuning. The $TE_{-2,3}$ mode is supressed in turn by the $TE_{+2,3}$ mode which has stronger coupling to the beam for the present beam diameter as is manifested in Fig. 3 by the slightly lower threshold current for the latter mode. To conserve computer time the beam energy risetime is much faster than the experimental value (~ 1 μsec). The slower risetime would probably allow TE_{03} mode operation to extend to slightly lower magnetic fields, and thus achieve slightly higher efficiency, than in the present calculations. After about 25 nsec an equilibrium with a single dominant mode is obtained. A single-mode equilibrium for this system was obtained in all cases simulated. The dominant mode obtained as a function of magnetic field is plotted in Fig. 4 for several beam currents. Figures 5 and 6 show a comparison of the calculated optimum efficiency and power, and optimum magnetic field with the experimental data of Kreischer et al. for the TE_{03} and TE_{23} modes. A map of the interacting modes under steady-state conditions as a function of magnetic field is shown in Fig. 7. The figure shows the $Q\times$ threshold beam power curves and the optimum efficiency QP_b as a function of magnetic field for the TE_{03} mode. It indicates that efficient operation of the TE_{03} mode can occur well into the magnetic field region where the TE_{23} modes have

lower starting currents and could be expected to limit TE_{03} mode operation. To facilitate comparison with other work, the calculated results for each mode are presented in terms of the normalized parameters ϵ and δ as shown in Fig. 8. The TE_{23} mode results correspond to the optimized single-mode case. The TE_{03} mode δ for each ϵ is limited by mode competition except for the highest and lowest ϵ values. However the highest efficiencies are obtained at the intermediate ϵ values. The mode density parameter $T_0 = 3.6$.

III-B $TE_{6,2,1}$ Mode Gyrotron Results

A high voltage, intense-beam gyrotron designed to operate in the $TE_{6,2,1}$ mode at 35 GHz has been extensively tested at NRL by Gold and co-workers.[1] $TE_{m,2}$ "whispering gallery" modes are desirable for their effective coupling to annular beams propagating near the cavity wall and their relative freedom from competition with other TE modes. This system has been extensively analyzed in the single-mode approximation[1] and it has also been simulated using a particle code.[12] The gyrotron design parameters used in the present calculations—which used a sinusoidal profile—include: an output Q factor of 250 for the $TE_{6,2}$ mode, a cavity length of 4 cm, a maximum cavity wall radius $r_w = 1.6$ cm, a beam guiding center radius $R_0 = 1.16$ cm, and a beam velocity pitch ratio $\alpha = 1$. Calculations were carried out as a function of magnetic field for a beam energy of 735 keV and beam current of 1600 A. To approximate the finite risetime of the electron gun voltage, the beam energy was ramped up, linearly, from 500 keV to the maximum value, 735 keV, during the first 5 nsec of the simulation. To approximate space-charge-limited emission operation of the cathode, the beam current was scaled as the 4/3 power of the beam energy. To approximate the effect of the pump magnet on the beam, the beam velocity pitch ratio was increased linearly during the beam energy ramp-up.

Although there are several non-$TE_{m,2,1}$ cavity modes with resonant frequencies near the $TE_{m,2,1}$ mode, particularly the $TE_{10,1,1}$ and $TE_{1,4,1}$ modes, these have weaker coupling to the beam than the $TE_{m,2,1}$ type modes for the chosen beam position and therefore competition is expected to occur only between modes of the latter type. These modes are approximately

equally spaced so that a three-mode interaction characterized by: $2\omega_n - \omega_{n-1} - \omega_{n+1} \approx 0$, can occur. This is also the dominant mode interaction process in the quasi-optical gyrotron.[8] Five-mode simulations with $-8 \leq m \leq -4$ were carried out to investigate the effect of mode-competition. The negative sign for m indicates a mode rotating counter to the sense of electron gyration.[1] The choice of negative m's was dictated by the beam position. The output Q factors for the other $TE_{m,2,1}$ modes were estimated by scaling the $TE_{6,2,1}$ mode Q factor by the square of the resonant frequency. The effect of competition between the two rotational polarizations is treated separately below.

The time evolution of the mode output powers is shown in Fig. 9 for a magnetic field of 2.75 T. As expected from the change in cyclotron frequency during the voltage ramp, the initial interaction is with the $TE_{-7,2,1}$ mode.[1] The $TE_{-6,2,1}$ mode becomes dominant as the peak voltage is reached. The principal competing modes are the $TE_{-7,2,1}$ and $TE_{-5,2,1}$ modes, consistent with the three-mode interaction model. These modes are not suppressed completely, but achieve an equilibrium at a power level of about 3% of the dominant mode. The mode density parameter $T_0 = 2.7$ for this configuration.

The equilibrium output power as a function of magnetic field is shown in Fig. 10. The experimental data has been normalized to a peak power of 100 MW. The particle simulation code results obtained by Lin et al. are also shown.[12] The present calculations show the transition from the $TE_{-5,2}$ to the $TE_{-6,2}$ mode occurring at about 2.47 T, the peak $TE_{-6,2}$ efficiency (18%) occurring at about 2.55 T, and the transition from the $TE_{-6,2}$ to the $TE_{-7,2}$ mode occurring at about 2.77 T. The magnetic field range of $TE_{-6,2}$ mode operation obtained by the present calculations are shifted up by about 8% relative to the experimental data. This discrepancy may be due to approximations in the theory such as the neglect of self-fields or beam temperature, to calibration errors in the experimental voltage or magnetic field, or to differences between the experimental and theoretical voltage pulse and velocity pitch ratio. In particular, the diode voltage waveform was highly transient in this experiment, and an accurate measurement of beam voltage as a function of time was difficult to achieve. In order to understand the physics, this has been simulated as a 5 nsec

ramp from 500 to 735 kV, followed by a period of constant voltage which was not present in the experiment. The calculated peak $TE_{-6,2}$ mode efficiency and optimum magnetic field agree well with the simulation results of Lin et al., but the $TE_{-5,2}$ to $TE_{-6,2}$ mode transition obtained by Lin et al is shifted up about 4% compared to the present results (or about 12% relative to the data. The particle code results are less single-moded in that significant power is obtained in the $TE_{-5,2}$ mode well into the magnetic field range in which $TE_{-6,2}$ mode is dominant. The reason for this difference is not clear. The two theoretical approaches agree in the single-mode approximation[12] and, although the numerical methods are very different, the main difference in the physical models is that the Lin theory uses a self-consistent (non-fixed) profile for the mode axial structure in the cavity. One would expect this feature to affect the single-mode as well as the multimode results.

An interesting effect observed in the NRL experiment was the generation of azimuthal "standing" modes, that were observed in a breakdown cell, and could be used as a diagnostic for the radial and azimuthal structure of an operating mode.[1] The generation of clear standing patterns was easily achieved experimentally by placing the electron beam at a radius for which the coupling was approximately equal to the co-rotating and counterrotating polarizations of a particular $TE_{\pm m,2}$ mode. In order to understand this effect, calculations have been carried out to investigate the competition between the two circular polarizations of the $TE_{6,2,1}$ mode as a function of the radius of the annular beam. It was found, as expected, that the polarization with the stronger coupling to the beam suppresses the other polarization so that the equilibrium state should have a single polarization. On the other hand, the rate of suppression is slow for almost equal coupling so that both polarizations could be present in a short pulselength experiment. This effect is shown in Fig. 11 and is consistent with the NRL experiment.[1] The calculated equilibrium or near equilibrium mode output power is shown as a function of beam radius in Fig. 12 along with the $\pm m$ mode coupling coefficient.

IV Discussion and Conclusions

A fully nonlinear, time-dependent, multimode theory has been formulated for waveguide cavity gyrotrons and applied to two configurations which have been investigated experimentally. The calculations, although lengthy, can be feasibly carried out on a fast computer such as the Cray. The agreement obtained between theory and experiment is good for the MIT 140 GHz gyrotron considering that the results are sensitive to the beam α which was not characterized experimentally. Better agreement might also be obtained by using the more realistic Gaussian axial RF field profile in the cavity instead of the sinusoidal profile. Qualitative agreement between theory and experiment was obtained for the NRL 35 GHz intense-beam gyrotron experiment. Multimode effects were found to cause little reduction in the peak efficiency of either configuration. The equilibrium state of the MIT gyrotron was always single-moded. A single transverse mode dominated the equilibrium states of the NRL gyrotron, but the competing modes were not entirely suppressed. This lack of total suppression may be a feature of the three-mode interaction which occurs in the latter configuration. The mode density parameter $T_0 \sim 3$ for both configurations. Gyrotrons currently under development have much values of this parameter and may be more limited by multimode effects.

V Acknowledgment

This work was supported by the Office of Naval Research. The calculations were supported by a Naval Research Laboratory Cray Production Runs grant.

References

1. S.H. Gold, A.W. Fliflet, W.M. Manheimer, R.B. McCowan, W.M. Black, R.C. Lee, V.L. Granatstein, A.K. Kinkead, D.L. Hardesty, and M. Sucy, *Phys. Fluids* **30**, 2226 (1987).

2. K.E. Kreischer, private communication.

3. B. van der Pol, *Philos. Mag.* **3**, 65 (1927).

4. W.E. Lamb, Jr., *Phys. Rev.* **134**, A1429 (1964).

5. M. Sargent, M.O. Scully, and W.E. Lamb, Jr., *Laser Physics* (Addison–Wesley: Reading, Mass., 1974), chap. 8.

6. M.A. Moiseev and G.S. Nusinovich, *Izv. Vyssh. Uchebn. Zaved., Radiofiz.* **17**, 1709 (1974) [*Radiophys. Quantum Electron.* **17**, 1305, (1976)].

7. G.S. Nusinovich, *Int. J. Electron.* **51**, 457 (1981).

8. T. Antonsen, B. Levush and W.M. Manheimer, submitted to *Phys. Fluids B.*

9. A. Bondeson, W.M. Manheimer and E. Ott, in *Infrared and Millimeter Waves*, edited by K.J. Button, (Academic Press, 1983), Vol. 9, Chapter 7.

10. O. Dumbrajs, G.S. Nusinovich and A.B. Pavelyev, *Int. J. Electron.* **64**, 137 (1988).

11. E. Borie and B. Jödicke, *IEEE Trans. Plasma Sci.* **16**, 116 (1988).

12. A.T. Lin, C.-C. Lin, Z.H. Yang, K.R. Chu, A.W. Fliflet, and S.H. Gold, *IEEE Trans. Plasma Sci.* **16**, 135 (1988).

13. K.E. Kreischer, J.B. Schutkeker, B.G. Danly, W.J. Mulligan, and R.J. Temkin, *Int. J. Electron.* **57**, 835 (1984).

14. A.W. Fliflet, *Int. J. Electron.* **61**, 1049 (1986).

15. A.W. Fliflet, M.E. Read, K.R. Chu, and R. Seeley, *Int. J. Electron.* **53**, 505 (1982).

16. A.W. Fliflet and W.M. Manheimer, *Phys. Rev. A* **39** 3432 (1989).

17. T.M. Tran, B.G. Danly, K.E. Kreischer, J.B. Schutkeker, and R.J. Temkin, *Phys. Fluids* **29**, 1274 (1986).

18. B.G. Danly and R.J. Temkin, *Phys. Fluids* **29**, 561 (1986).

19. *Handbook of Mathematical Functions*, ed. by M. Abramowitz and I.A. Stegun, (*Dover Publications, Inc.*: New York) chap. 25 (1970).

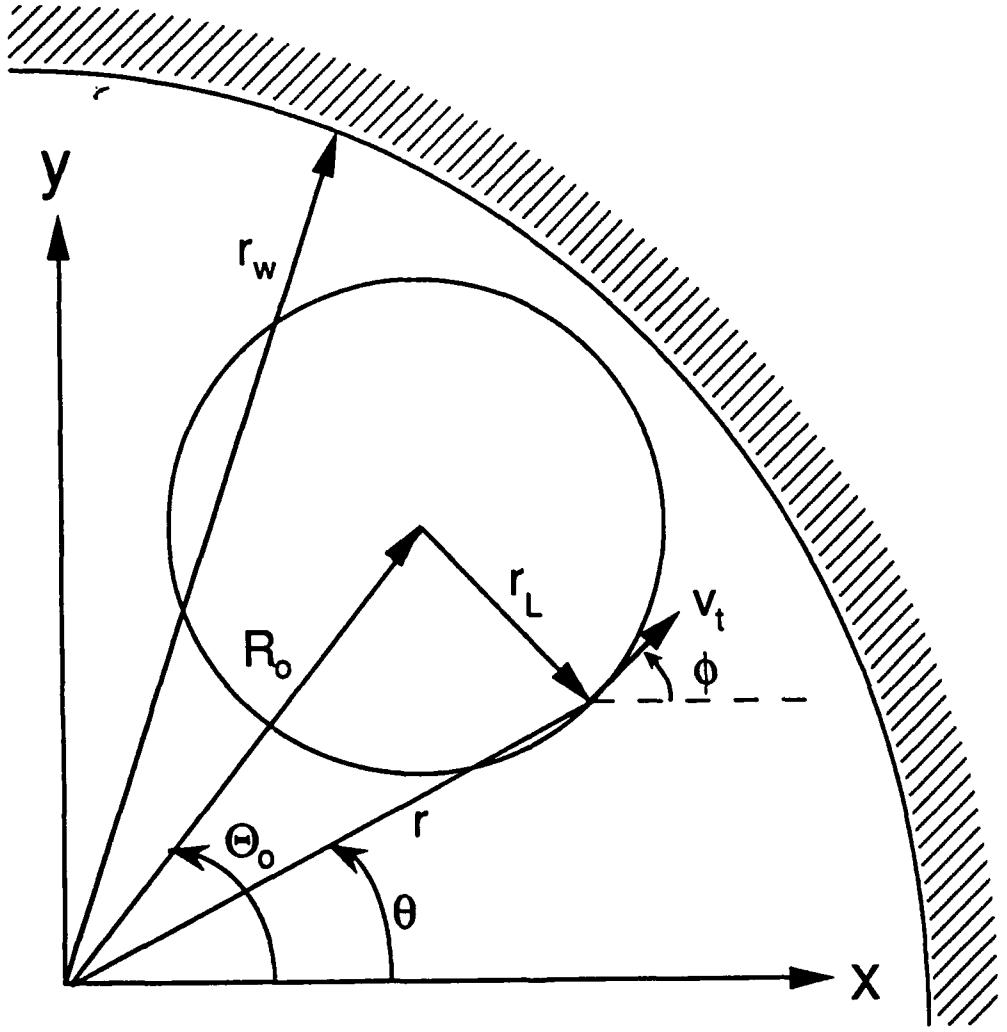

Fig. 1 — Cross-sectional geometry of the gyrotron cavity and electron orbits

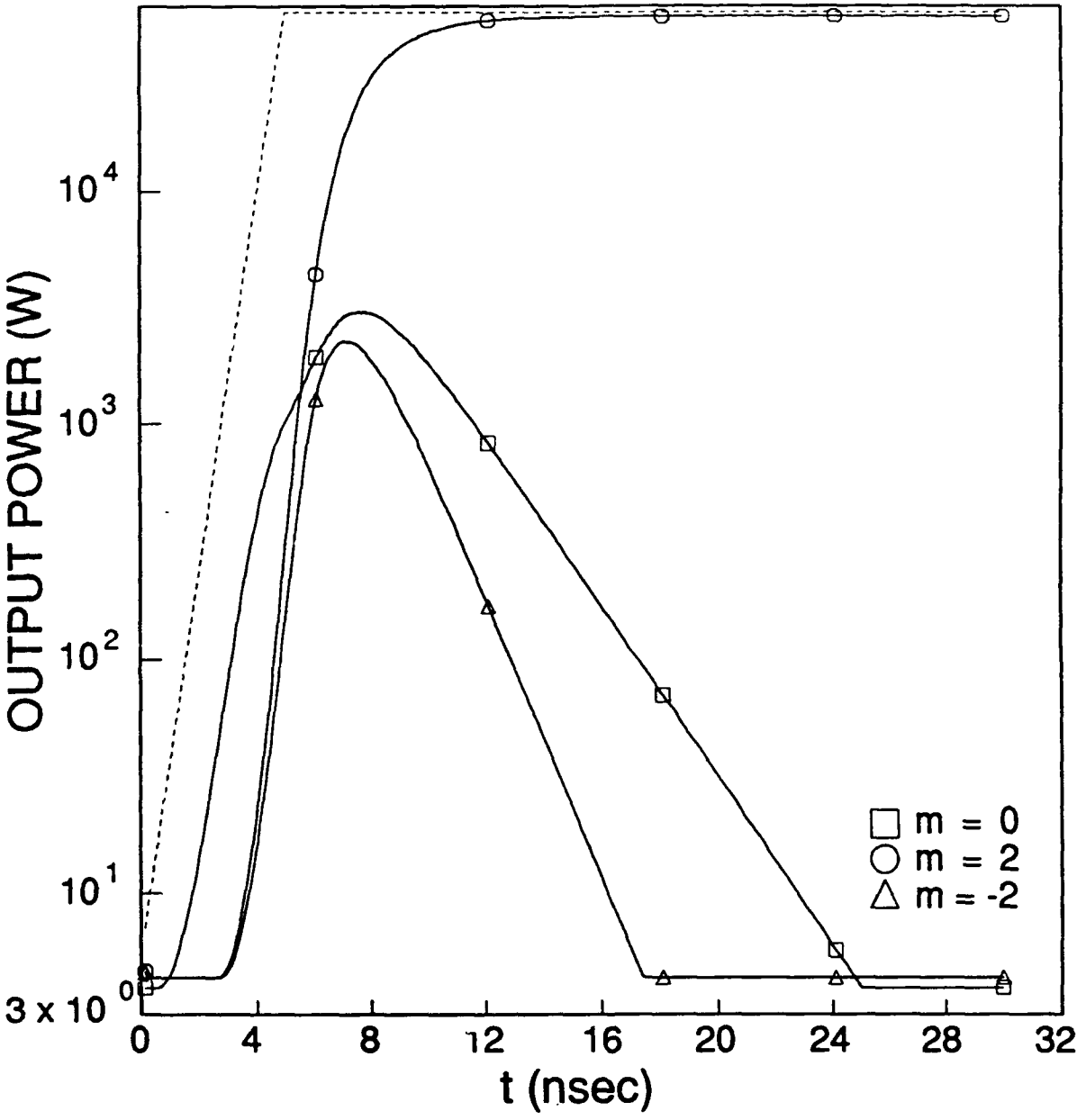

Fig. 2 — Time evolution of mode output powers for the TE_{m3} modes of the MIT 140 GHz gyrotron

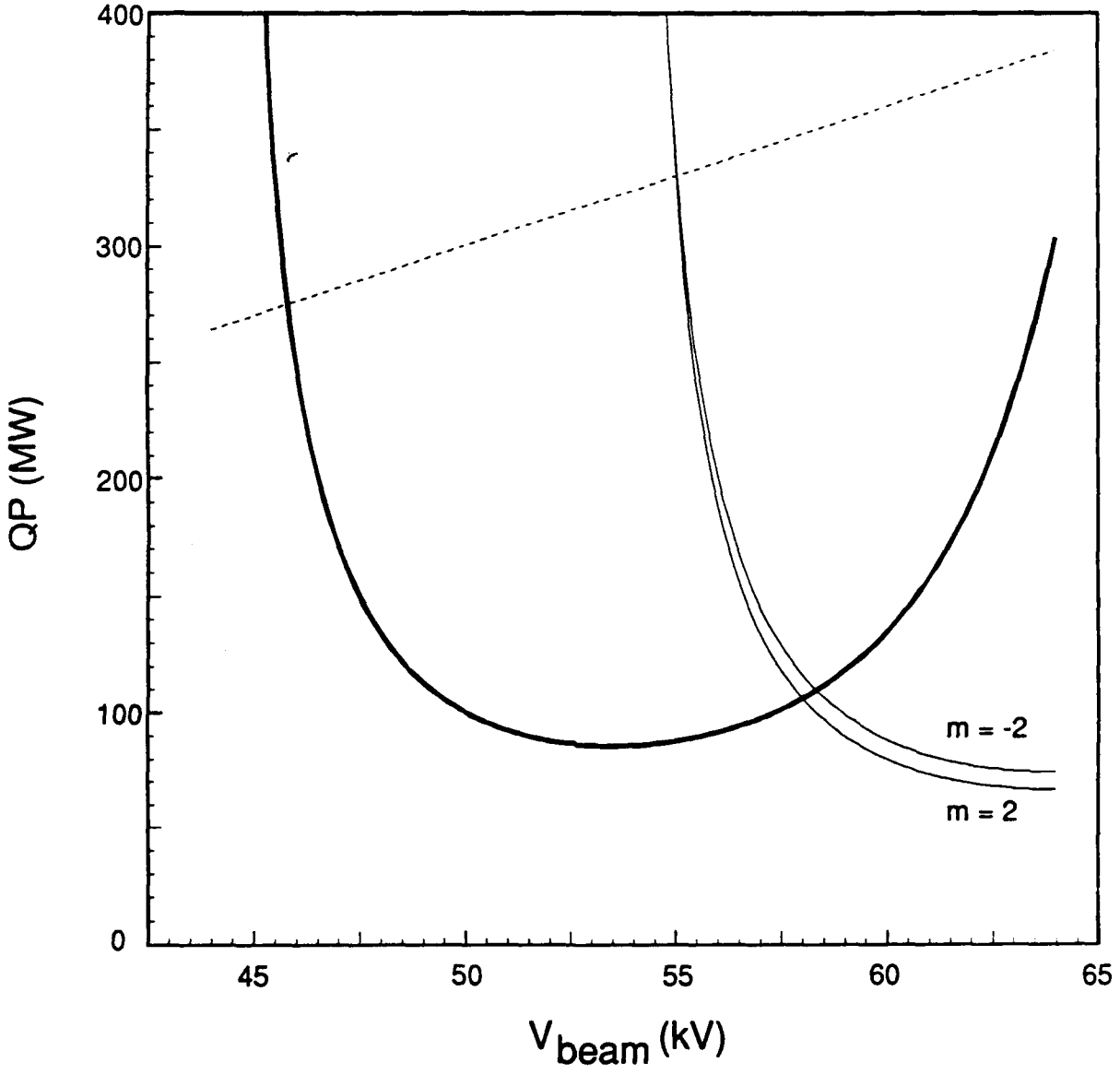

Fig. 3 — $Q \times$ (threshold beam power) for the TE_{03} and TE_{23} modes as a function of gun voltage

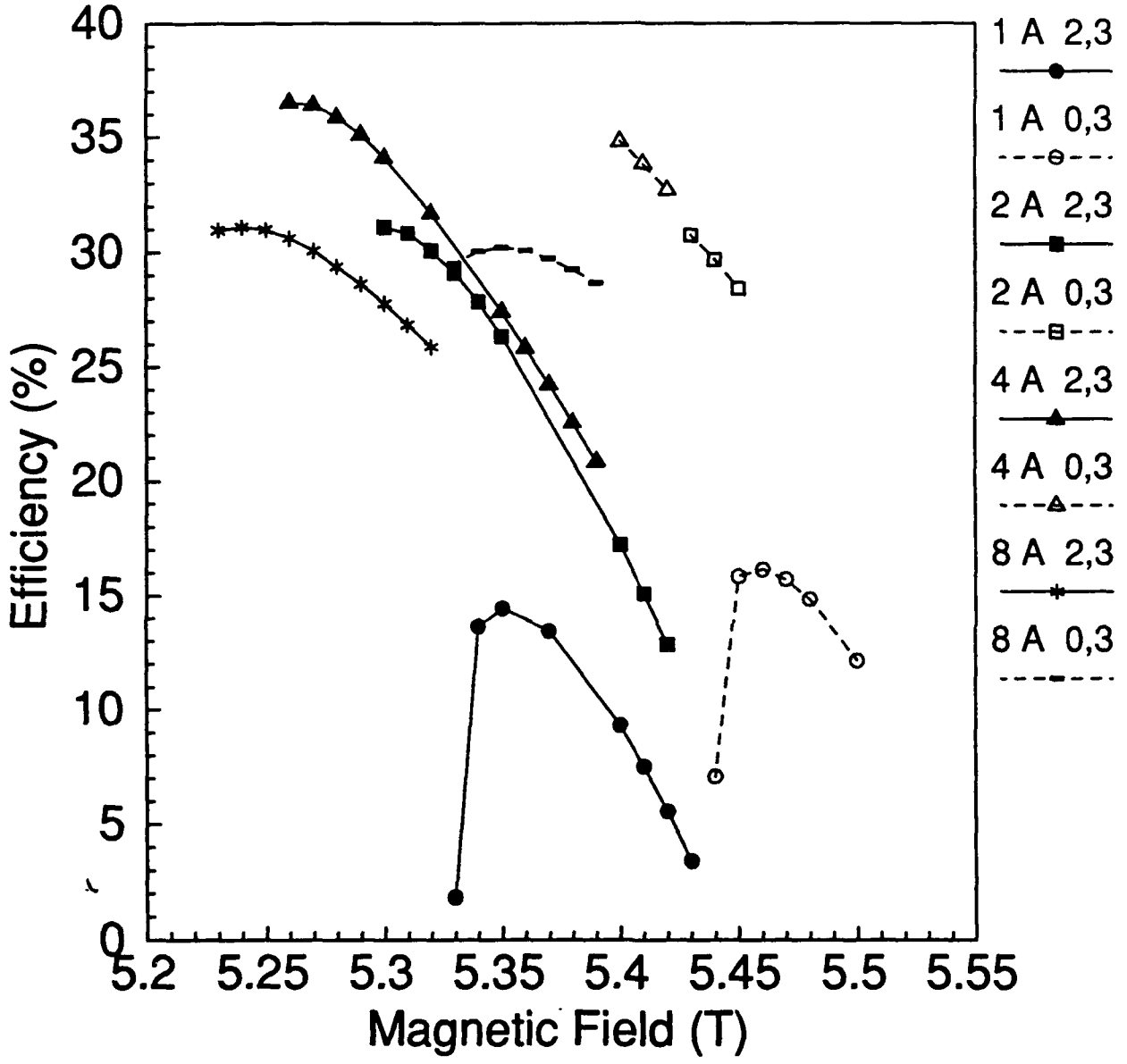

Fig. 4 — Efficiency of dominant steady-state mode as a function of magnetic field for the MIT 140 GHz gyrotron

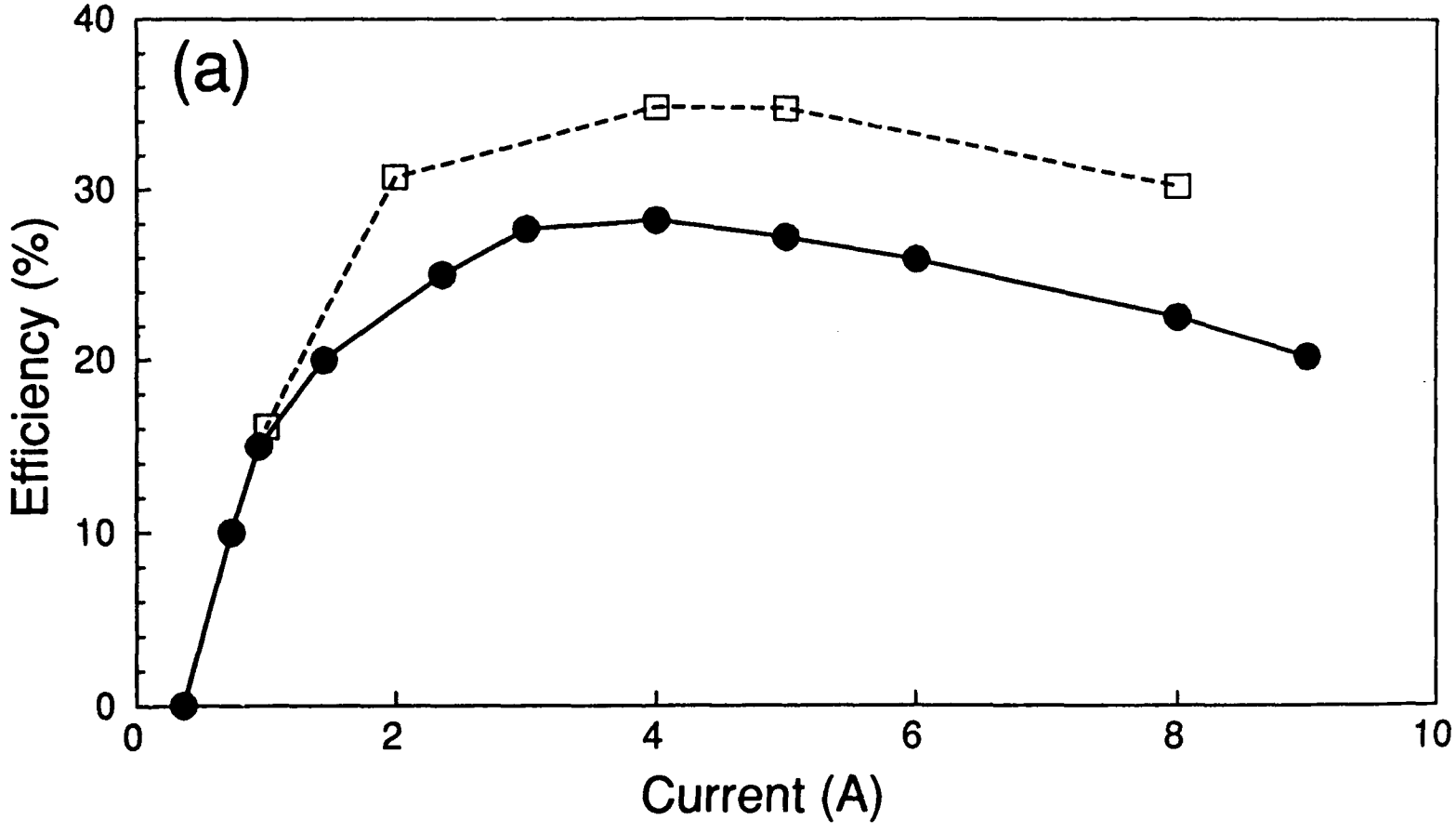

(a)

Fig. 5 — Comparison of calculated and experimental results for TE_{03} mode operation of the MIT gyrotron: (a) efficiency, and (b) optimum magnetic field. The solid dots show the experimental data[2] and the open squares show the calculated results.

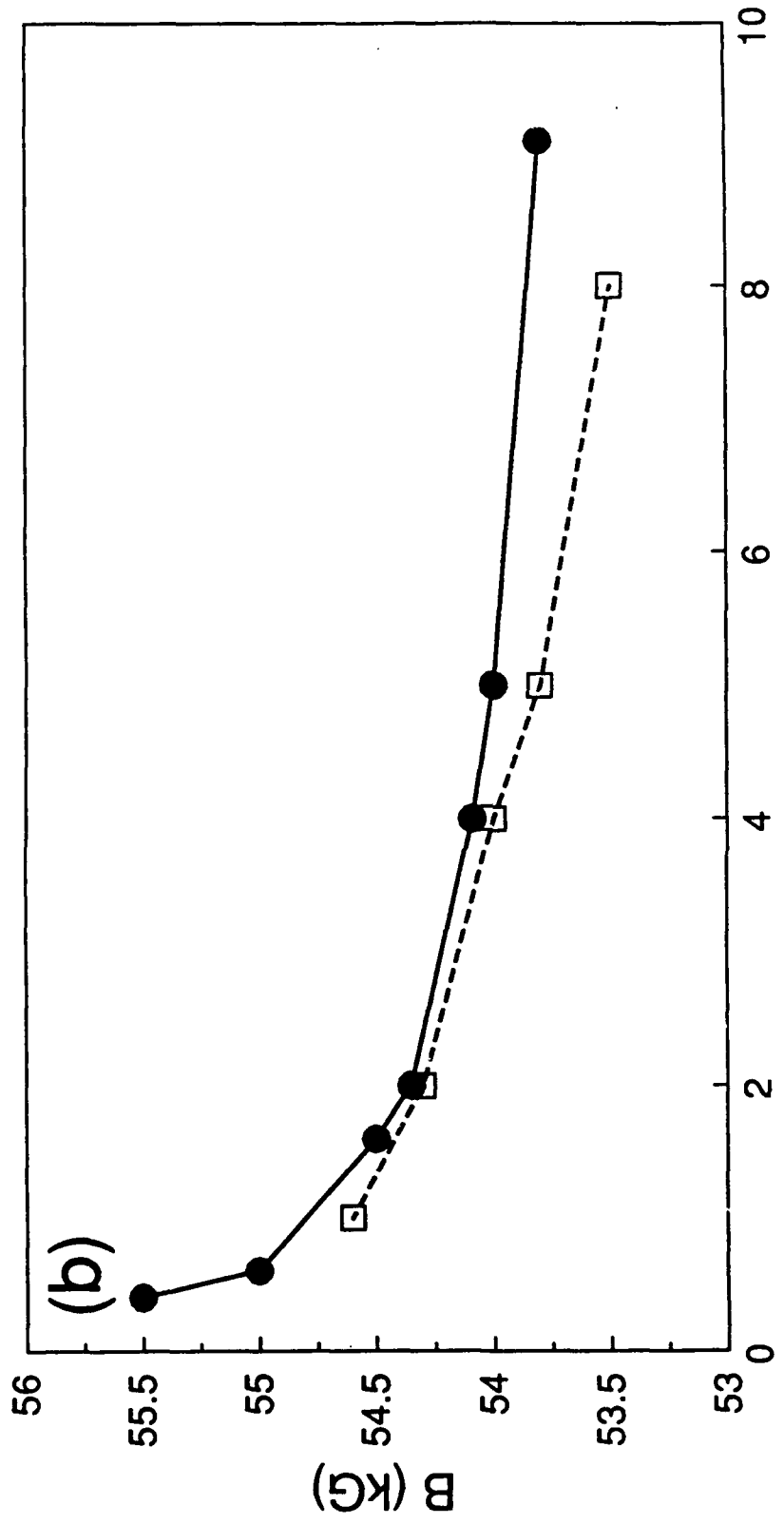

(b)

Fig. 5 — (Continued) Comparison of calculated and experimental results for TE_{01} mode operation of the MIT gyrotron: (a) efficiency, and (b) optimum magnetic field. The solid dots show the experimental data[2] and the open squares show the calculated results.

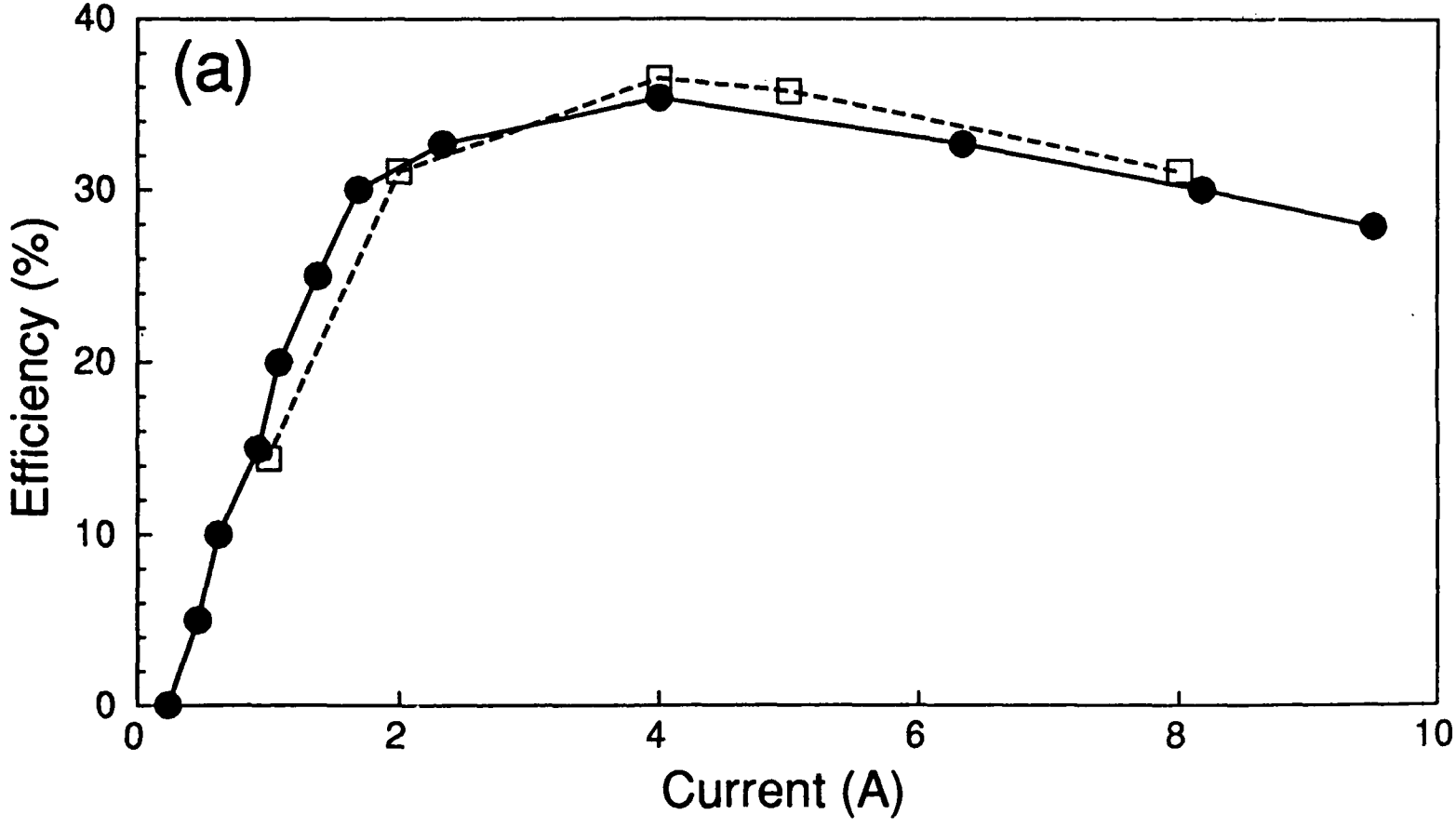

(a)

Fig. 6 — Comparison of calculated and experimental results for TE_{23} mode operation of the MIT gyrotron: (a) efficiency, and (b) optimum magnetic field. The solid dots show the experimental data[2] and the open squares show the calculated results.

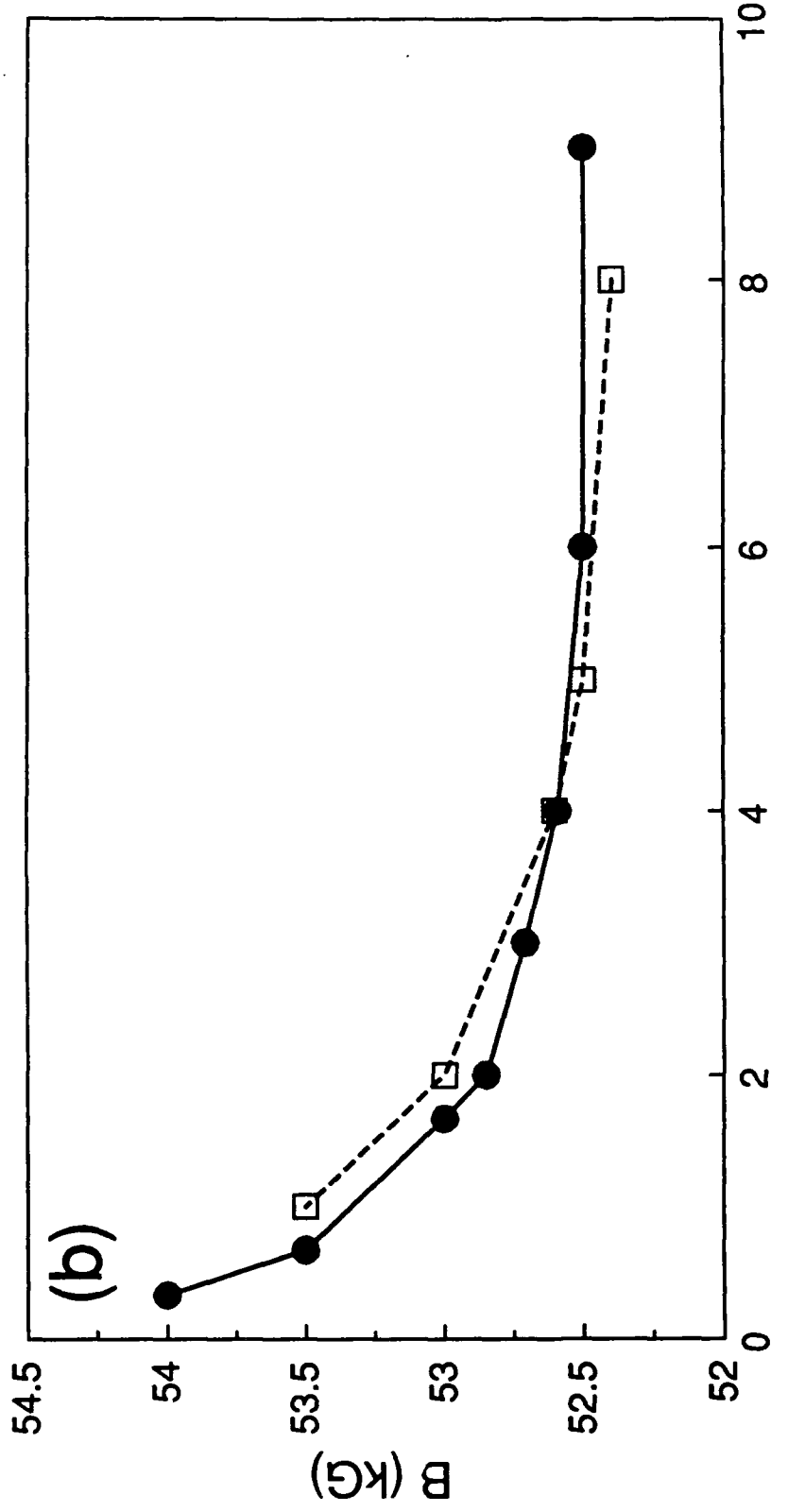

(b)

Fig. 6 — (Continued) Comparison of calculated and experimental results for TE_{23} mode operation of the MIT gyrotron: (a) efficiency, and (b) optimum magnetic field. The solid dots show the experimental data[2] and the open squares show the calculated results.

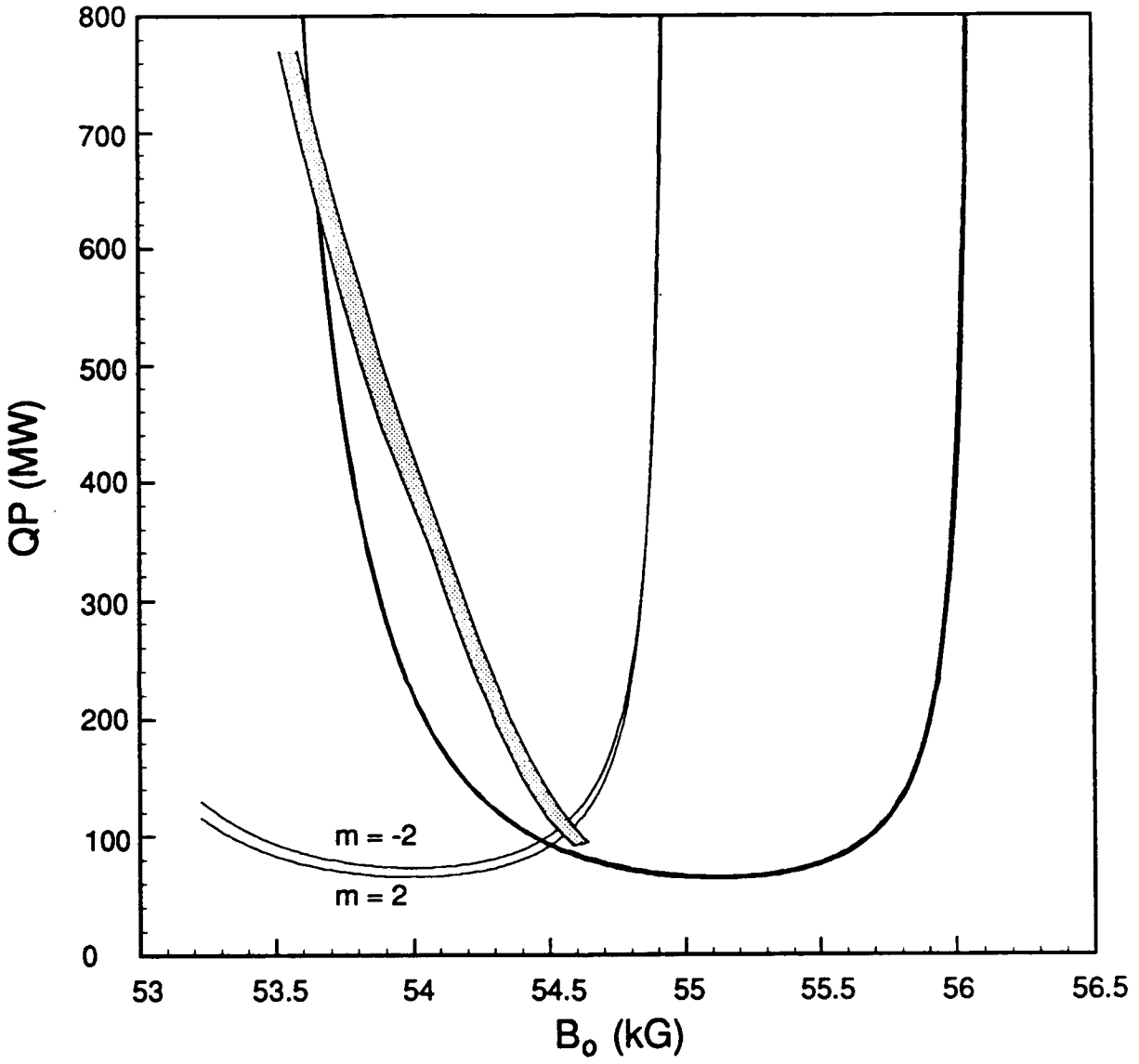

Fig. 7 — Predicted regions of TE_{03} and TE_{23} mode oscillations in the Q × (output power) — magnetic field plane. The optimum efficiency operating points for the TE_{03} mode are indicated by the shaded region

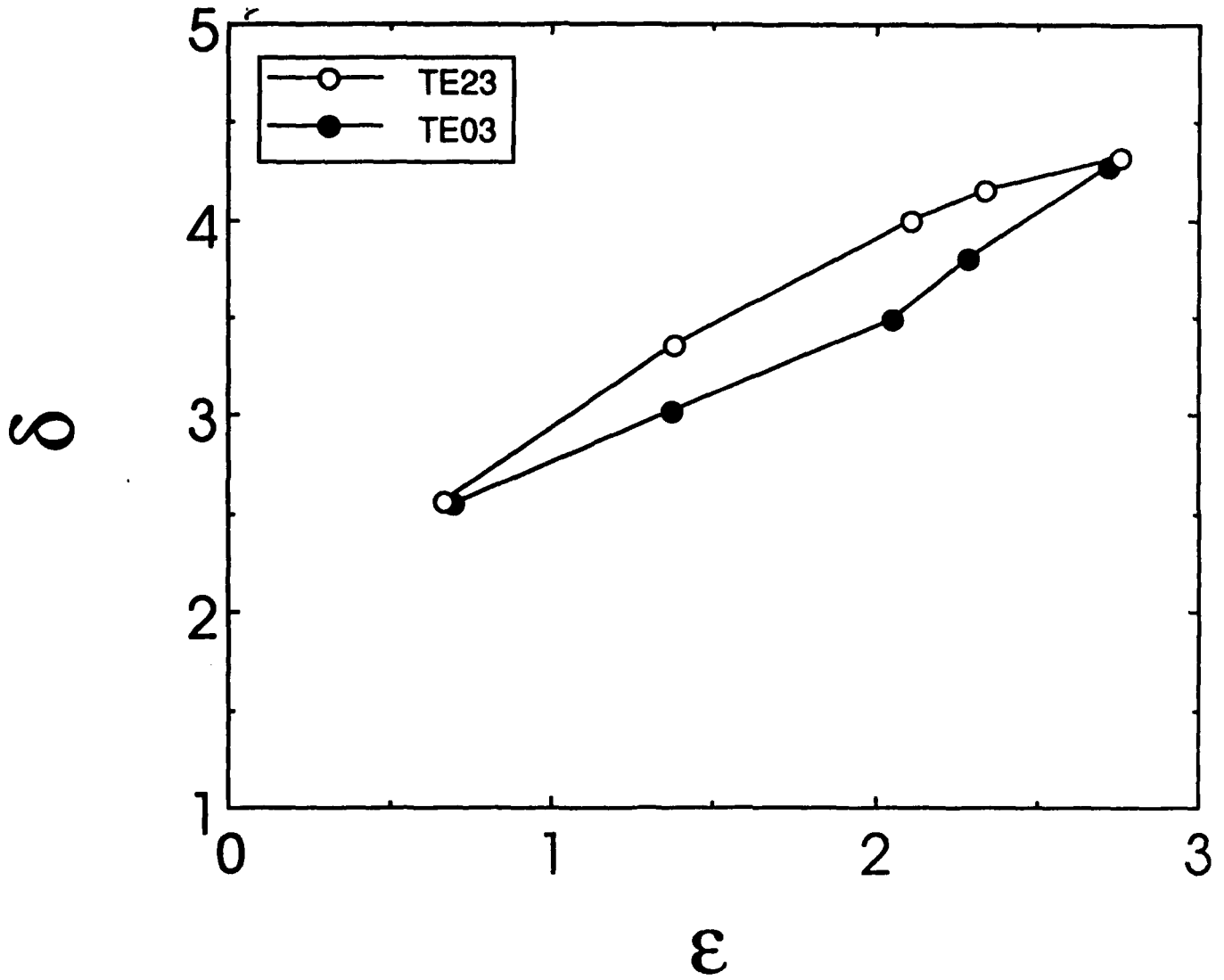

Fig. 8 — Optimum efficiency operating points. TE_{23} mode results are indicated by the open circles and the TE_{03} mode results are indicated by the solid dots.

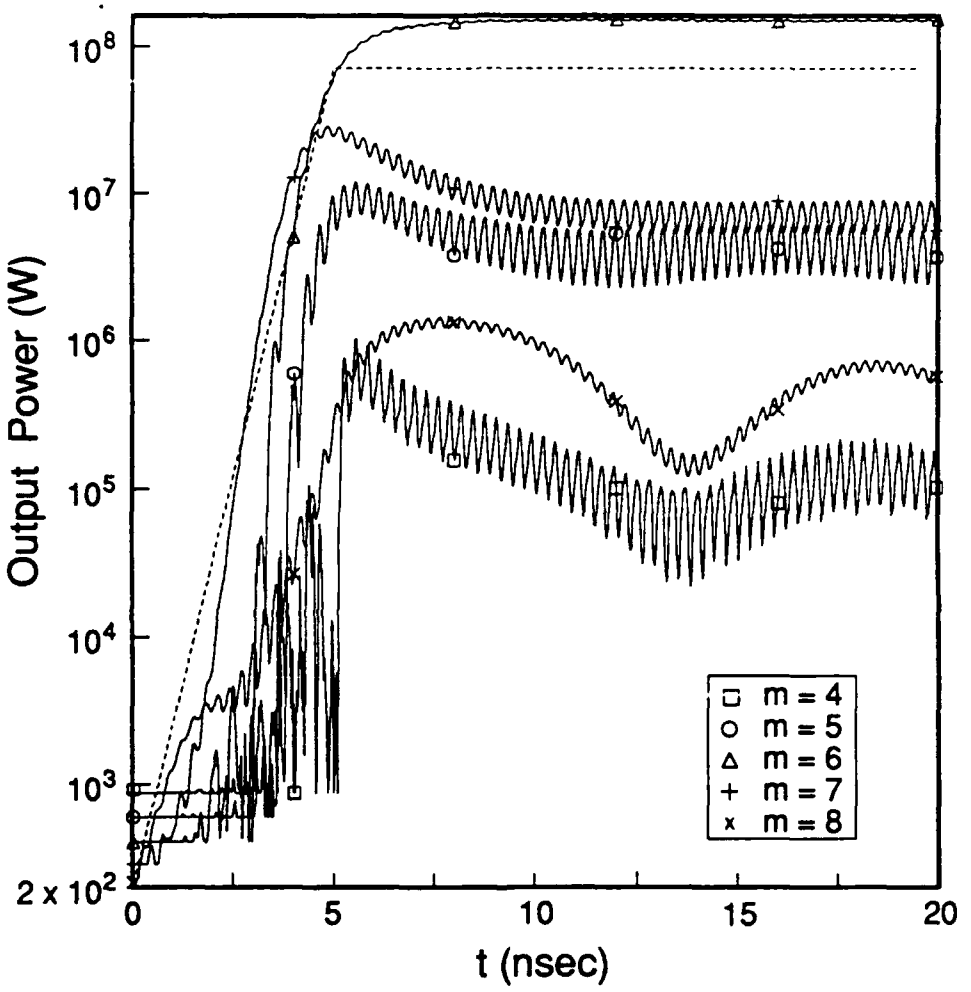

Fig. 9 — The time evolution of the TE_{-m2} mode output powers for the NRL gyrotron for a magnetic field of 2.75 T.

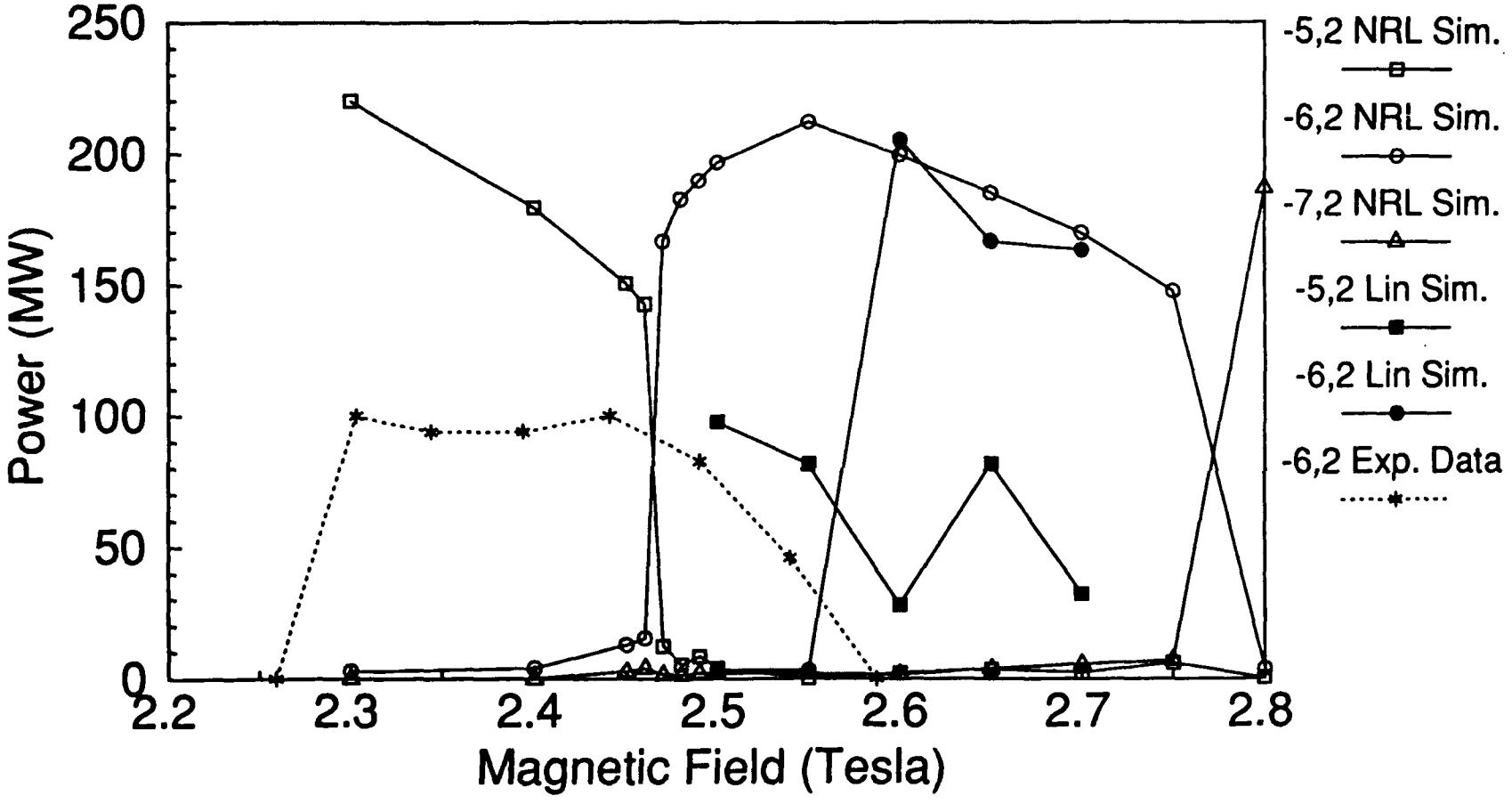

Fig. 10 — Equilibrium mode output power as a function of magnetic field. The open symbols indicate the present theoretical results, the closed symbols indicate the theoretical results of Lin *et al.*[12], and the asterisks denote the TE_{62} mode experimental data.[1] The squares denote $m = -5$ results, the circles denote $m = -6$ results, and the triangles denote the $m = -7$ results.

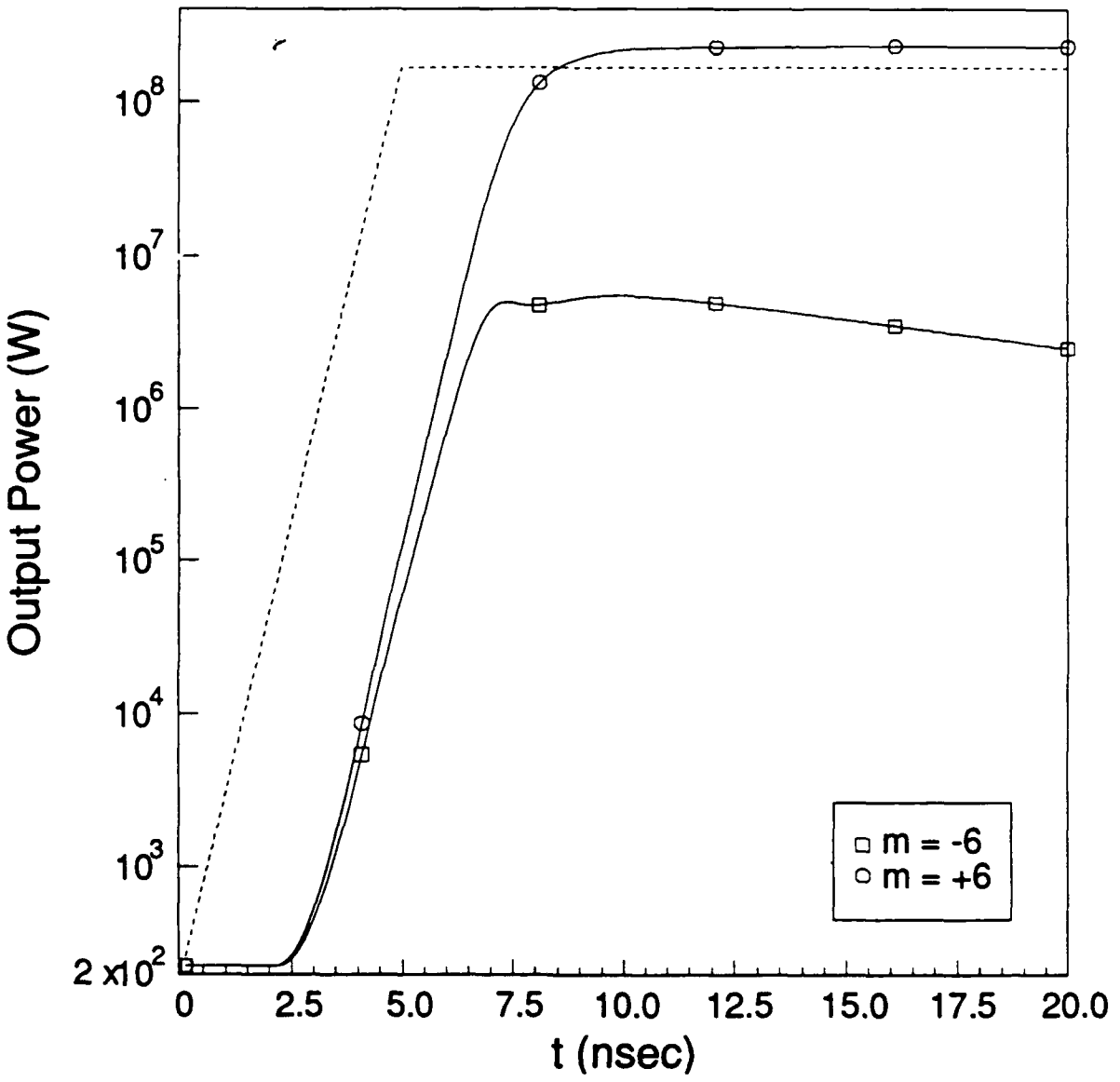

Fig. 11 — Time evolution of the two rotating $TE_{6,2,1}$ modes for a beam radius of r_b = 1.02 cm which corresponds to near equal coupling. The magnetic field is 2.6 T.

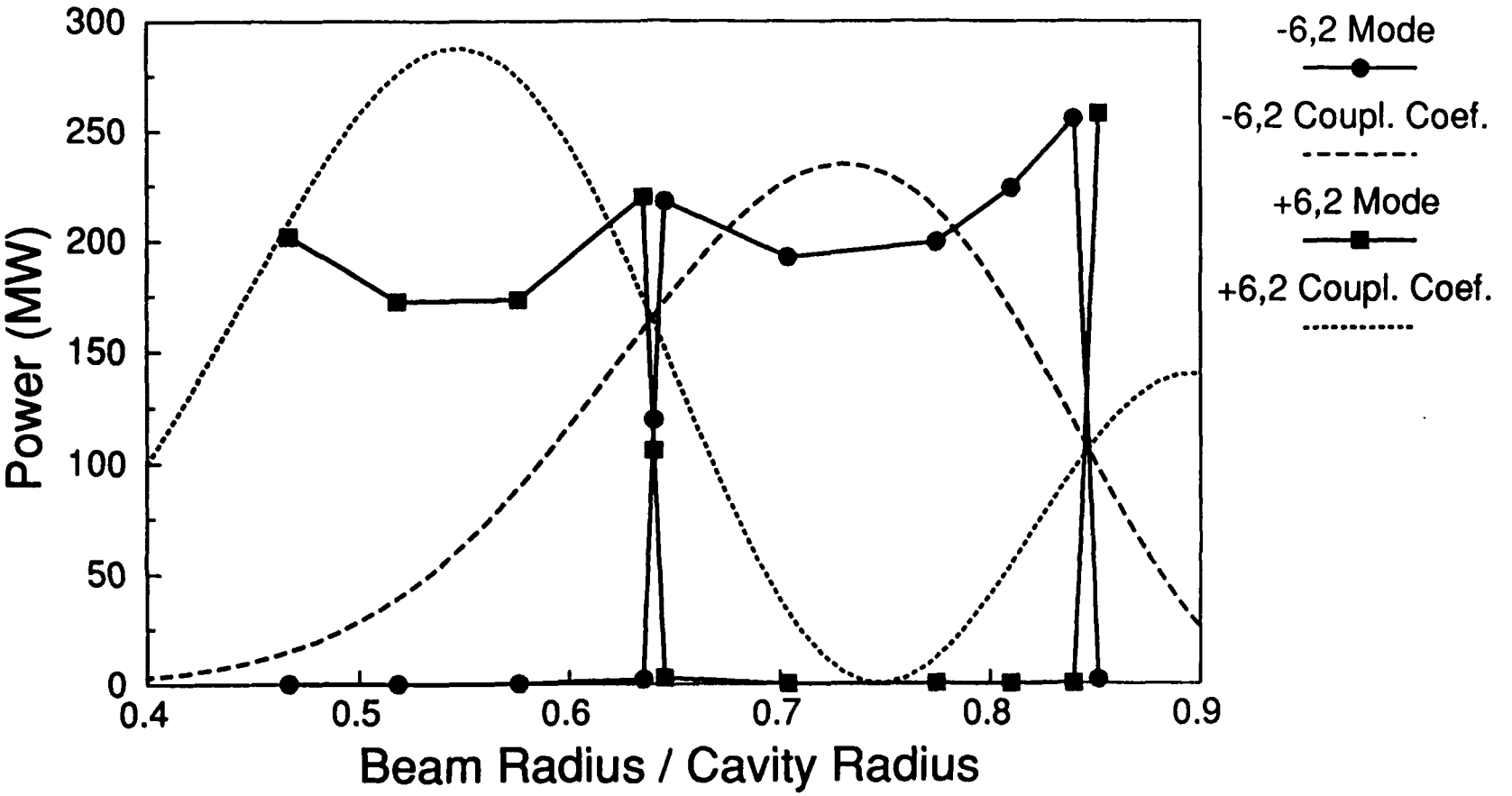

Fig. 12 — Equilibrium $TE_{\pm 6,2,1}$ rotational mode output power as a function of electron beam radius for a magnetic field of 2.6 T. The circles show the $TE_{-6,2,1}$ mode power and the squares show the $TE_{+6,2,1}$ mode power. The dashed curve with the longer dasheds indicates the $TE_{-6,2,1}$ mode coupling coefficient and the curve with the shorter dashes indicates the $TE_{+6,2,1}$ mode coupling coefficient.